One-step in situ synthesis and characterization of $W_{18}O_{49}$@carbon coaxial nanocables

Yuqin Zhou, Yong Zhang, and Ruying Li
Department of Mechanical and Materials Engineering, University of Western Ontario, London, Ontario, Canada N6A 5B9

Mei Cai
General Motors Research and Development Center, Warren, Michigan 48090-9055

Xueliang Sun[a)]
Department of Mechanical and Materials Engineering, University of Western Ontario, London, Ontario, Canada N6A 5B9

(Received 25 November 2008; accepted 4 February 2009)

We demonstrate here in situ synthesis of bulk yield $W_{18}O_{49}$@carbon coaxial nanocables based on an easily controlled chemical vapor deposition process at relatively low temperature (760 °C) using metallic tungsten powder and ethylene (C_2H_4) as the raw materials. Transmission electron microscope (TEM), energy dispersive x-ray (EDX), and x-ray diffraction (XRD) analyses indicate that the resultant nanostructures are composed of single-crystalline $W_{18}O_{49}$ nanowires, coaxially covered with amorphous carbon walls. A vapor–solid (VS) mechanism is proposed to interpret the formation of the nanocables. The effect of carbon sources on the nanocable growth was investigated. The results revealed that the introduction of carbon species not only causes the production of $W_{18}O_{49}$@C nanocable structures, but also obviously modulates growth behaviors and core/shell diameter ratio of the nanocables. The obtained nanocables may find great applications in catalyst systems and optical and electronic nanodevices because of their enhanced surface properties and in high chemical stabilities.

I. INTRODUCTION

One-dimensional (1D) nanostructures have drawn intensive research interest because of their unique applications in mesoscopic physics and nanoscaled devices.[1–3] To tailor the physical and chemical properties of 1D nanostructures to a more diverse range, one of the most effective ways is to create heterostructures with different compositions and interfaces.[4–6] Among various 1D heterostructures, the coaxial nanocable structure has become a significant class because of their wide applications in field effect transistors,[7,8] light emitting diodes,[9] solar cells,[10] gas sensors,[11] magnetic sensors[12] and optical[13–17] nanodevices.

More recently, the synthesis of coaxial structures consisting of a carbon shell and a semiconductor or metallic core has become an emerging research field because of the distinct properties combining of carbon nanotube and other functional materials. Since 1D nanostructures can be easily oxidized and contaminated because of their high surface chemical reactivity, leading to the deterioration of their performance, a carbon shell can provide an effective layer to ensure the stabilization and passivation of the active nanocore surface. To date, various metal[18–23] or semiconductor[24–31] @carbon coaxial nanocable structures have been developed, which raise some new research interest as a result of their distinct physical and chemical properties. As reported previously, Sn@carbon nanocables have been successfully synthesized by chemical vapor deposition,[18] and the nanocables have exhibited excellent stability as a catalyst support for fuel cells.[32]

Monoclinic $W_{18}O_{49}$ is a transitional oxide semiconductor exhibiting unique shear plane structural defects[33] and potential applications such as gas sensors and field emitters in the nanoregime.[34–36] Synthesis of $W_{18}O_{49}$ nanowires and nanorods has been investigated by thermal treatment,[37] vapor transport,[38] wet chemical[39] and electron-beam-induced methods.[40] However, there is a gap in the synthesis of $W_{18}O_{49}$@carbon coaxial nanocable structures in open literature. In this paper, we report the synthesis of bulk yield $W_{18}O_{49}$@carbon nanocables via a simple one-step in situ chemical vapor deposition technique under ambient pressure. In addition, we investigated effects of carbon species on the formation of the nanocables and proposed a growth mechanism.

[a)]Address all correspondence to this author.
e-mail: xsun@eng.uwo.ca
DOI: 10.1557/JMR.2009.0214

II. EXPERIMENTAL DETAILS

High-purity monocrystalline W powder (0.20 g, 99.9+%, 0.6–1 μm in diameter, Sigma-Aldrich, Inc., St. Louis, MO), was held at the bottom of a ceramic boat, and then the boat was placed in the middle part of a quartz tube in a conventional horizontal tube furnace. Prior to heating, the quartz tube was purged with high purity argon (99.999%) at a flow rate of 200 sccm (standard cubic centimeters per minute) for 20 min. After that, the system was heated to 760 °C at a heating rate of 50 °C/min under different atmospheres, including (a) Ar + H_2O, (b) Ar + H_2O + CH_3OH, and (c) Ar + H_2O + C_2H_4. The sample was then kept at the reaction temperature for 3 h before cooling down to room temperature. After the experiment, the starting black metallic tungsten powder has changed into dark purple-blue chunks.

The samples were characterized by Hitachi S-4500 field-emission scanning electron microscope (FESEM; Tokyo, Japan) operated at 5.0 kV, Bruker D8 micro x-ray diffractometer (XRD; Madison, WI), JEOL 2010F transmission electron microscope (TEM; Tokyo, Japan) operated at 200 kV, and Oxford INCA energy dispersive x-ray spectroscope (EDX; UK) operated at 10 keV.

III. RESULTS AND DISCUSSION

Figure 1 shows general morphology of the tungsten oxide nanowires grown under different atmospheres. Figure 1 (a_L) shows a typical low-magnification image of the tungsten oxide nanowires without the introduction of carbon species. The high-magnification image in Fig. 1 (a_H) reveals aggregated growth of the nanowires possessing irregular cross-section shape, which is similar to the bundled $W_{18}O_{49}$ nanowires reported previously.[41] The diameter of the nanowires ranges from tens of nanometer to about 400 nm, and the length ranges from several hundreds of nanometers to approximately 2 μm.

Keeping the other processing parameters the same, methanol (CH_3OH) and ethylene (C_2H_4) were introduced into the gas streams respectively as the carbon species. When methanol was introduced into the growth process, only trivial improvement was observed in elevating the growth rate and obtaining a narrower size distribution, as shown in Fig. 1 (b_L) and (b_H). However, when C_2H_4 was introduced as the carbon species at a flow rate of 3 sccm, the nanowires exhibited a dramatic change in both growth rate and aspect ratio. The SEM images in Fig. 1 (c_L) and (c_H) indicate that the free-

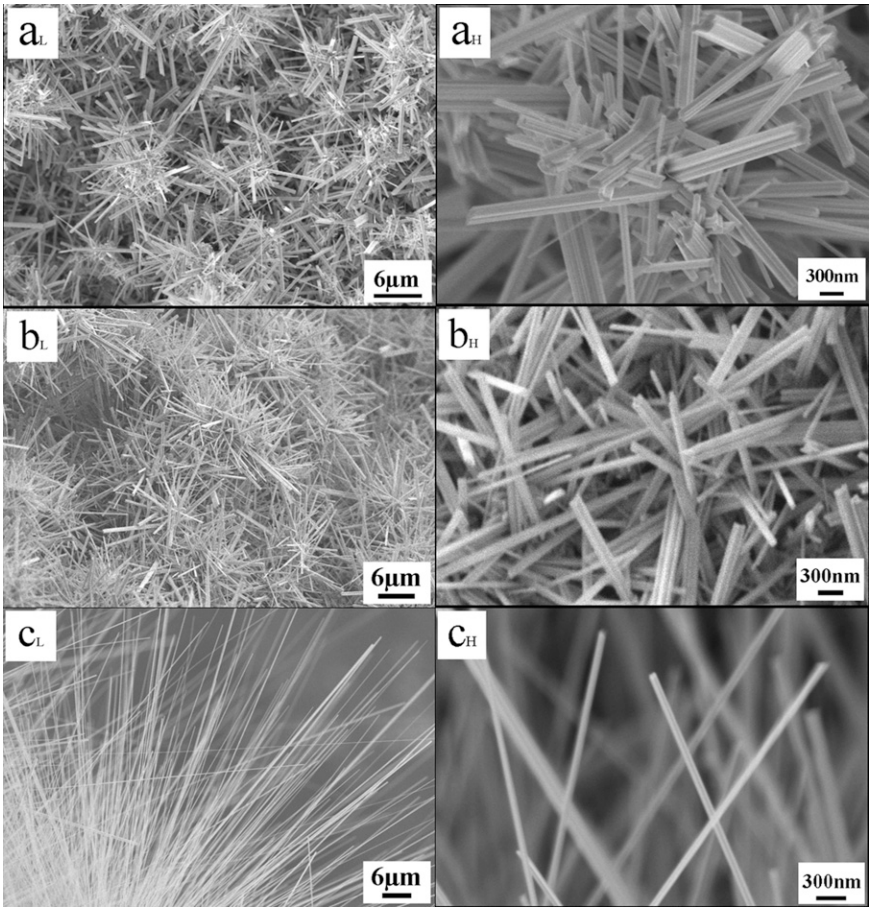

FIG. 1. SEM images of tungsten oxide nanowires grown under different atmosphere (a) Ar + H_2O, (b) Ar + H_2O + CH_3OH, and (c) Ar + H_2O + C_2H_4.

standing nanowires are thin and uniform. Compared with the product obtained without the introduction of carbon species, the diameter of all the nanowires is much smaller, from 20 to 100 nm. Low-magnification SEM observations reveal that length of the nanowires is about 50 μm, which is more than 10 times longer than those grown without introducing C_2H_4. At the reaction temperature used in our experiments, C_2H_4 decomposes into atomic carbon species and hydrogen[42] while methanol is supposed to decompose firstly into $\cdot CH_3$ and $\cdot OH$ radicals.[24] The final morphology of the nanostructures differs between the samples by introducing ethylene or methanol, probably because of the differences in the reaction atmosphere.

Figures 2(a) and 2(b) show x-ray diffraction pattern of the sample synthesized under the atmospheres of Ar + H_2O or Ar + H_2O + C_2H_4. Sharp diffraction peaks in Fig. 2(a) were identified as monoclinic $W_{18}O_{49}$ (JCPDS No. 05-0392), and diffraction peaks of tungsten can also be observed as a result of the residual metallic tungsten powder. Diffraction peaks in Fig. 2(b) can also be indexed as monoclinic $W_{18}O_{49}$. Further, the high relative intensity of the peak at $2\theta = 23.5°$ indicates oriented growth of the nanowires along the ⟨010⟩ crystal direction. On the other hand, no obvious tungsten peaks were observed, indicating that the reaction from tungsten to tungsten oxide was more complete because of the introduction of C_2H_4. In addition, the full width at half-maximum (FWHM) of the diffraction peaks in Fig. 2(b) tends to be wider compared with the case in Fig. 2(a), indicating smaller diameter of the nanowires.

To gain the microstructural insight of the nanowires, TEM observation was carried out as shown in Fig. 3. Figures 3(a) and 3(b) show the typical TEM bright-field images of a single nanowire after C_2H_4 was introduced. Evidently, the nanostructure consists of a core/shell structure with a dark core and light outer layer. Scrutiny of the core/shell nanostructure shows that the thickness of the carbon layer is around a couple of nanometers, and the diameter of the dark core is about 20 nm. Figure 3(c) shows the high-resolution TEM image of a nanowire. The lattice spacing of about 0.38 nm corresponds to the *d* value of (010) lattice fringes of $W_{18}O_{49}$, indicating that the nanowire grew along the ⟨010⟩ direction of the monoclinic structure. The carbon layer exhibits amorphous characteristics, which may be another reason why the diffraction peaks of carbon covered $W_{18}O_{49}$ were broadened. Figure 3(e) shows the selected-area electron diffraction (SAED) pattern of the nanowire, the indexed SAED pattern reveals that the nanowire grows along ⟨010⟩ direction, which is consistent with the HRTEM observation. Further, the streaked pattern of the SAED indicates the presence of oxygen deficiencies that are commonly observed in tungsten oxides.[43] EDX spectrum of the nanowires was shown in Fig. 3(e), where tungsten, oxygen, and carbon signals were detected.

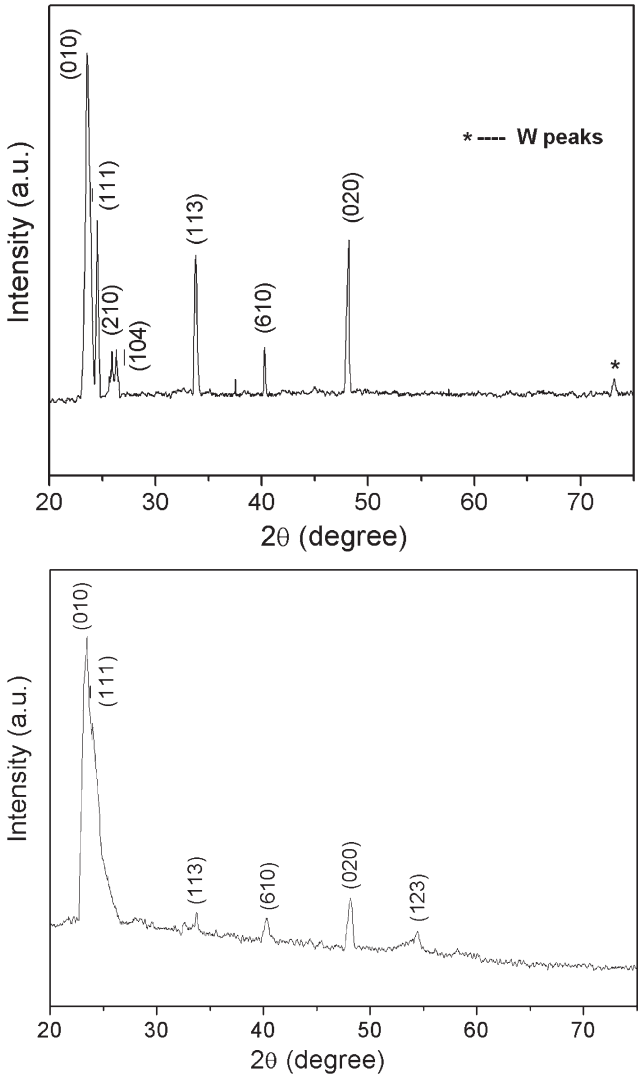

FIG. 2. X-ray diffraction pattern of the samples synthesized under the atmosphere of (a) Ar + H_2O or (b) Ar + H_2O + C_2H_4.

Based on the aforementioned results, the introduction of carbon not only induces the production of carbon-coated nanocables, but also significantly affects the morphology of the final products. Therefore, the effects of the carbon amount on the growth of nanowire have been further investigated. Figure 4 shows the diameter and length dependency of nanowires on the flow rate of C_2H_4. Even when the flow rate of C_2H_4 was as low as 1 sccm, as shown in Fig. 4(a), significant changes were observed both in diameter and length of the nanowires. Compared with pure $W_{18}O_{49}$ nanowires obtained without C_2H_4, the length of $W_{18}O_{49}$ nanowires increases up to 30 μm and the diameter decreases to less than 200 nm with the addition of C_2H_4. Nevertheless, there is still a

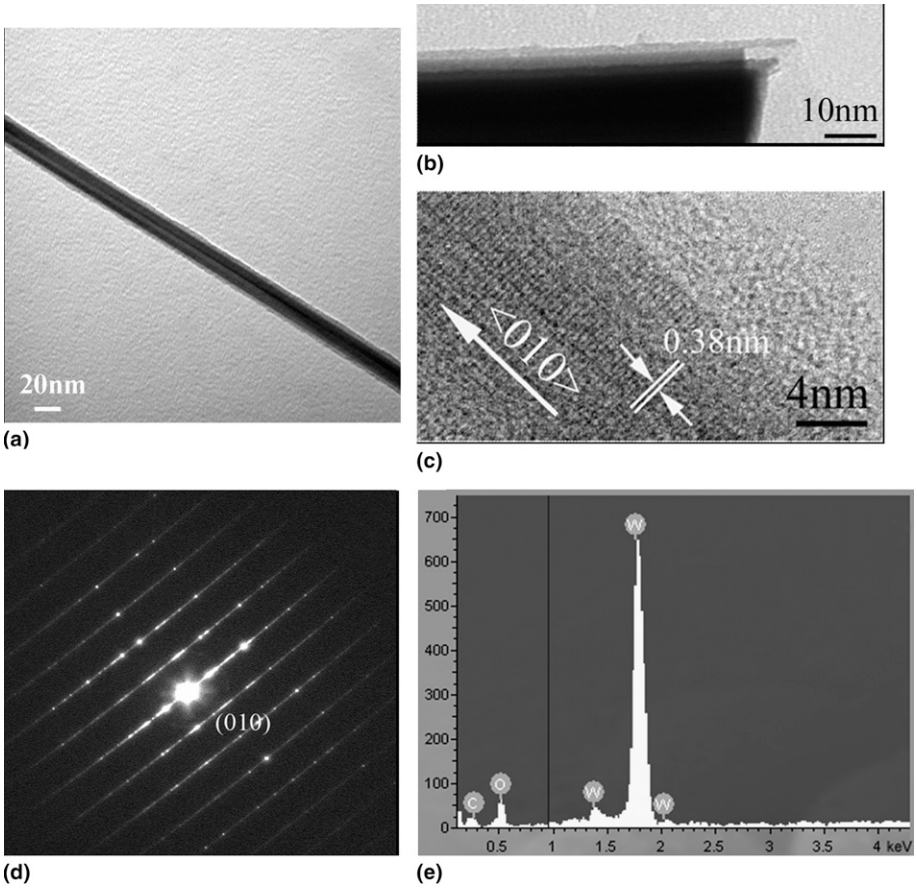

FIG. 3. (a, b) Typical TEM bright-field image, (c) HRTEM image, and (d) selected area electron diffraction pattern, (e) EDX of a single $W_{18}O_{49}$@C nanocable.

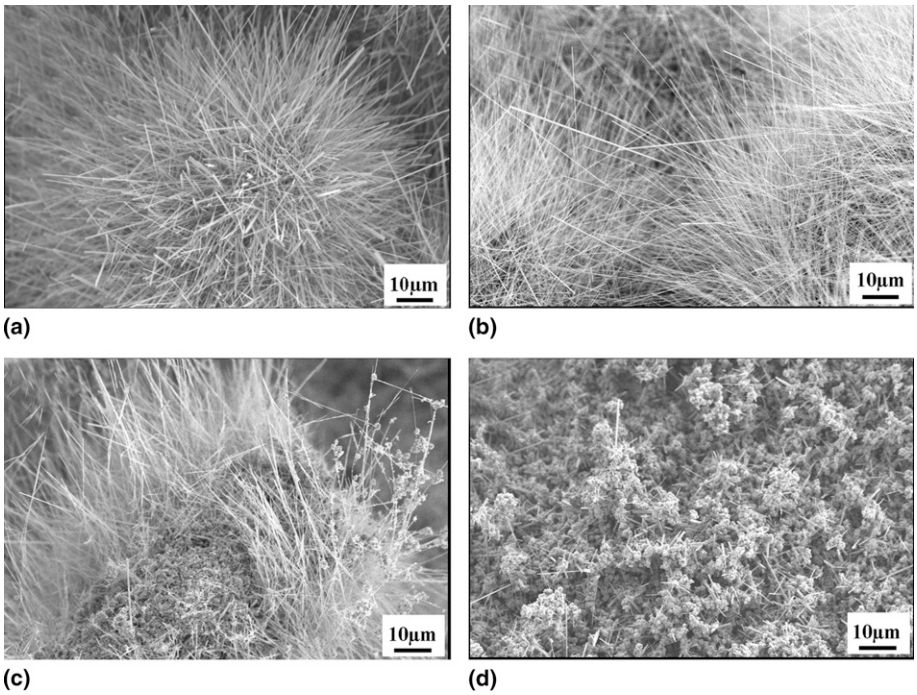

FIG. 4. SEM images of the $W_{18}O_{49}$@C nanocables under different C_2H_4 flow rates (a) 1 sccm, (b) 3 sccm, (c) 5 sccm, and (d) 7 sccm.

wide range distribution in diameters. As the flow rate of C_2H_4 was increased to 3 sccm, the length of nanowires further increased while the diameter decreased to 20–100 nm and exhibited more uniform distribution. When the flow rate of C_2H_4 was further increased to 5 sccm, the obtained nanowires became thicker and less uniform. In addition, some large aggregated particles (diameter > 1 μm) were found on the nanowires. When the flow rate was elevated to 7 sccm, the morphology of the product exhibited as a mixture of thicker nanorods and particles, revealing that excess ethylene had restrained the nanowire growth. These results suggest that the growth of nanowire is very sensitive to the carbon content in the reaction atmosphere. As shown in Table I, the correlation between the nanowires growth and the C_2H_4 flow rate is briefly summarized.

Figures 5(a)–5(d) show TEM images of the thickness of the carbon layer on the nanowires grown at flow rates of C_2H_4 of 1, 3, 5, and 7 sccm, respectively. While C_2H_4 was introduced at a flow rate as low as 1 sccm, as shown in Fig. 5(a), no obvious carbon layer is observed. When a moderate flow rate of C_2H_4 (3–5 sccm) was used, an evident carbon shell could be observed on the surface of nanowire with a thickness of several nanometers, as shown in Figs. 5(b) and 5(c). With further increasing of the flow rate of C_2H_4 to 7 sccm, the thickness of the carbon layer was significantly increased to above 10 nm, as shown in Fig. 5(d). Therefore, the carbon shell became thicker and thicker with increasing flow rate of C_2H_4. In addition, scrutiny of the nanowires through TEM has indicated that the nanocables with close-tip were observed at high ethylene flow rate (7 sccm in this work). When the flow rate of ethylene was controlled below 7 sccm, TEM results revealed open tip of the nanocables. The cavity in Fig. 5(d) was formed as a result of the epitaxial growth of the carbon shell along the surface of the $W_{18}O_{49}$ core. With increasing flow rate of ethylene, the concentration of carbon species also increased, which speeded up the growth rate of carbon shell along the length direction of the nanocables. Finally, the epitaxial growth of the carbon shell may close the nanowire tip during the cooling process, and a cavity could be generated at the tip of the nanocable. It is interesting to address the growth mechanism of the $W_{18}O_{49}$@C nanocables to further control the structure of core and thickness of shell as well as to tailor their

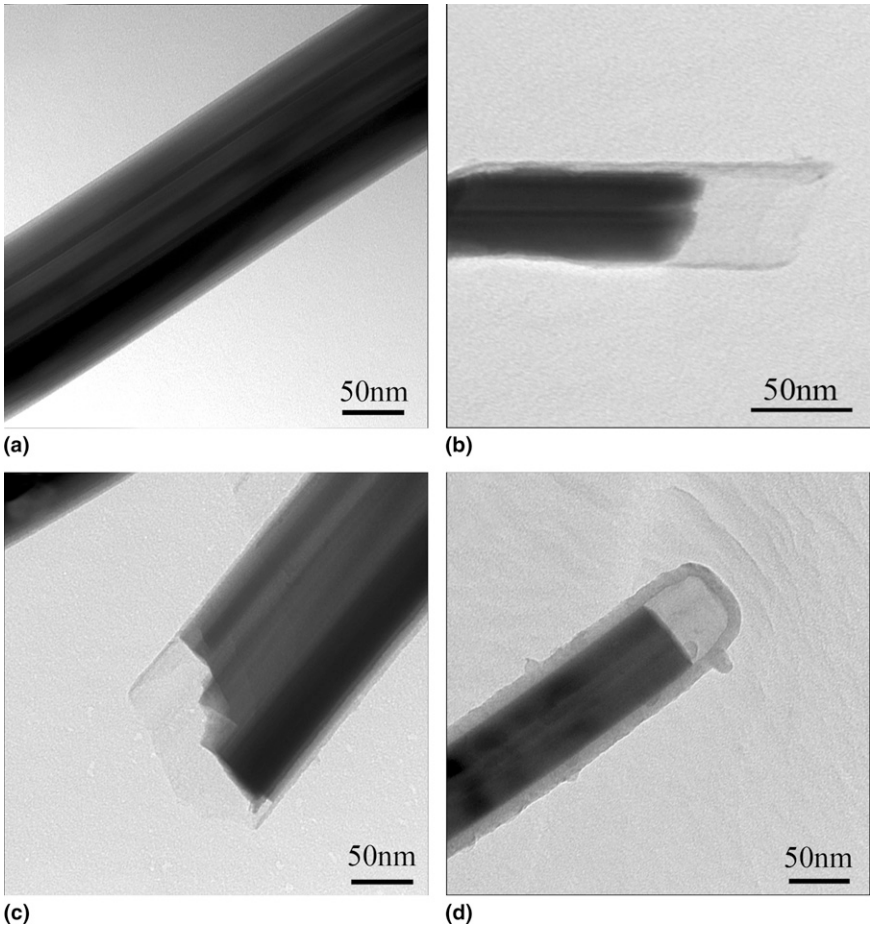

FIG. 5. TEM images of the $W_{18}O_{49}$@C nanocables under different C_2H_4 flow rates (a) 1 sccm, (b) 3 sccm, (c) 5 sccm, and (d) 7 sccm.

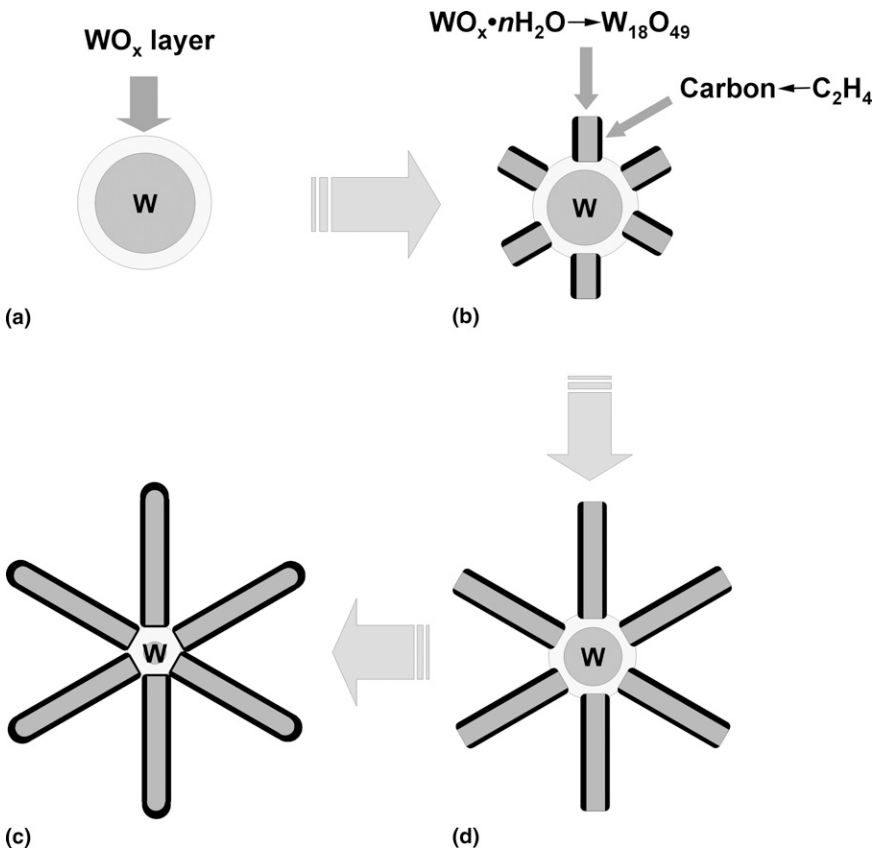

FIG. 6. Schematic diagram illustrating the growth mechanism of the $W_{18}O_{49}$@C nanocables.

properties. Electron microscopy scrutiny of the nanowires indicated that there were no other particles rather than WO_3 found at the tip or at the root of the nanorods, which differs from the VLS growth mechanism.[44]

We propose a vapor–solid (VS) growth mechanism here.[45] Basically the VS mechanism for metal oxide nanowire growth requires a low melting point metal or submetal oxide for the nanowire growth. In this work, it was hard to obtain tungsten vapor at such a low-growth temperature (760 °C) due to high melting point of tungsten (3422 °C). Although growth details of tungsten oxide nanowires still remain controversial, it is generally recognized that a tungsten oxide layer WO_x ($2 \leq x \leq 3$) was formed first on metallic tungsten particles.[46] In addition, it has been found that the growth of tungsten oxide nanowires can be significantly enhanced in the presence of water vapor.[47,48] The following reactions are proposed to dominate the growth of the $W_{18}O_{49}$ nanowires[46,49,50 51]:

$$\mathrm{W(s)} + x\mathrm{H_2O(g)} \leftrightarrow \mathrm{WO_x(s)} + x\mathrm{H_2(g)} \quad , \qquad (1)$$

$$\begin{aligned} &\Delta G_{1033\mathrm{K}} = -18.5\mathrm{kJ/mol}(x=2), \\ &\Delta G_{1033\mathrm{k}} = -10\mathrm{kJ/mol}(x=3)^{51} \\ &\mathrm{WO}_x + n\mathrm{H_2O} \leftrightarrow \mathrm{WO}_x{\cdot}n\mathrm{H_2O} \quad , \end{aligned} \qquad (2)$$

$$\mathrm{WO}_x{\cdot}n\mathrm{H_2O} + \mathrm{H_2} \leftrightarrow \mathrm{W_{18}O_{49}} + \mathrm{H_2O} \quad . \qquad (3)$$

When water vapor was introduced, a WO_x layer was formed as shown in reaction (1). Thermodynamic calculations of reaction (1) have been carried out based on the thermodynamic data in Ref. 51, revealing the spontaneous proceeding of the reaction. The introduction of water vapor could not only form the tungsten oxide, but also increase the rates of tungsten oxide evaporation and promote tungsten oxide hydrates formation ($WO_x{\cdot}nH_2O$) as shown in reaction (2). The supersaturation degree of the hydrate species was readily created because of their high volatility.[24] Subsequently, the decomposition of the volatile tungsten suboxide hydrate species allows the nucleation of localized $W_{18}O_{49}$ crystals as shown in reaction (3).[46]

In VS growth, the shape of the final crystal was determined by the surface energy of the growing surface planes.[52] For monoclinic $W_{18}O_{49}$ (JCPDS No. 05-0392), the lowest energy surfaces are likely the {010}-type surfaces,[36] and the initial formed tungsten oxide crystal clusters were inclined to be bounded by {010}-type facets. The tungsten oxide crystal clusters could act as the seeds for further crystal growth. The diffusion and decomposition of tungsten oxide hydrate species as

adatoms on the crystal clusters supported the elongated growth along the closed-packed ⟨010⟩ direction and finally resulted in the oriented growth of the tungsten oxide nanowires along ⟨010⟩ direction, as evidenced by XRD and HRTEM determination.

For the achievement of the $W_{18}O_{49}$@C nanocables, we assume that the carbon shell was generated accompanying the formation of tungsten oxide core as shown in Fig. 6. While the tungsten oxide nanorods were generated, the active carbon atoms were generated at the high-temperature reaction region because of the decomposition of C_2H_4. The freshly formed fine tungsten oxide nanorods would provide energetically favored sites for the adsorption of carbon atoms. Surface adsorption of the active carbon atoms could confine the radial growth of nanowires, and thinner nanowires were obtained. Simultaneously, the oriented, confined growth of thinner nanowires can decrease the consumption rate of volatile $WO_x{\cdot}nH_2O$ species, and keep the vapor pressure of $WO_x{\cdot}nH_2O$ at a relatively high level, which may accelerate the growth rate of nanowires. As a result, tungsten oxide nanowires with uniform, thinner diameter and longer length were obtained.

On the other hand, the tungsten oxide nanowires may promote the cracking of the carbon volatile species (C_2H_4) onto the nanowire surface[53]; in turn, the adsorption of carbon may decrease the energy barrier of further carbon deposition, forming a carbon shell on the surface of tungsten oxide nanowires as shown in Figs. 6(b) and 6(c). The growth of tungsten oxide core and carbon shell can occur simultaneously, providing sufficient availability of both tungsten and carbon sources, and finally results in the $W_{18}O_{49}$@C nanocable heterostructural geometry as shown in Fig. 6(d). A question may arise as to why the deposited carbon is amorphous rather than crystalline under these conditions. Obviously, hydrogen has been considered to play an important role in generating amorphous carbon nanotubes. Zhao et al.[54] reported that carbon atoms could easily form clusters before they meet the catalyst to form a crystalline structure using hydrogen as a carrier gas. Du et al.[55] reported the formation of amorphous carbon nanotubes as a result of the fast cooling rate of hydrogen because hydrogen has the highest thermal conductivity and the lowest density and dynamic viscosity[25] of all other conventional gases. In our case, the generation of hydrogen as shown in reaction (1) may produce ample hydrogen concentration that favors the amorphous carbon. Furthermore, tungsten and tungsten oxide are not good catalyst materials for the growth of carbon nanotubes compared with iron, cobalt, and nickel. Therefore, only amorphous carbon covered tungsten oxide nanowires were obtained in our study. Further investigation is underway to better understand these issues.

TABLE I. $W_{18}O_{49}$@C nanocable growth as a function of C_2H_4 flow rate.

C_2H_4 flow rate (sccm)	Length (μm)	Diameter (nm)	Qualitative remarks
1	30	>200	Less uniform
3	50	20–100	Uniform distribution
5	30	> 100	Less uniform
7	n/a	n/a	Rods and particles

IV. CONCLUSIONS

In conclusion, we have reported the one-step synthesis of $W_{18}O_{49}$@C coaxial nanocables via a simple vapor phase transport method under atmospheric pressure. The formation of the nanocable takes place via a vapor–solid (VS) process of growing $W_{18}O_{49}$ nanowires with the subsequent deposition of carbon. The results indicate that the careful control of source species and amount of source carbon not only enables the production of $W_{18}O_{49}$@C nanocable structure, but also results in a higher growth rate, smaller diameter, and more uniform size distribution. This method can be used to produce a wide range of materials and may have great applications in various nanostructured systems that require controlled physical and chemical properties, antioxidation protection and improved electrical conductivity, such as catalyst supports for fuel cells.

ACKNOWLEDGMENTS

This research was supported by General Motors of Canada, the Natural Science and Engineering Research Council of Canada (NSERC), Canada Research Chair (CRC) Program, Canadian Foundation for Innovation (CFI), Ontario Research Fund (ORF), Early Researcher Award (ERA), and the University of Western Ontario. We thank David Tweddell and Fred Pearson for fruitful discussion, structural characterization and special support.

REFERENCES

1. Y. Li, F. Qian, J. Xiang, and C.M. Lieber: Nanowire electronic and optoelectronic devices. *Mater. Today* **9,** 18 (2006).
2. Z.R. Dai, Z.W. Pan, and Z.L. Wang: Novel nanostructures of functional oxides synthesized by thermal evaporation. *Adv. Funct. Mater.* **13,** 9 (2003).
3. Y.N. Xia, P.D. Yang, Y.G. Sun, Y.Y. Wu, B. Mayers, B. Gates, Y.D. Yin, F. Kim, and Y.Q. Yan: One-dimensional nanostructures: Synthesis, characterization, and applications. *Adv. Mater.* **15,** 353 (2003).
4. M. Law, J. Goldberger, and P.D. Yang: Semiconductor nanowires and nanotubes. *Annu. Rev. Mater. Res.* **34,** 83 (2004).
5. G.C. Yi, C.R. Wang, and W.I. Park: ZnO nanorods: Synthesis, characterization and applications. *Semi. Sci. Tech.* **20,** S22 (2005).
6. A.J. Mieszawska, R. Jalilian, G.U. Sumanasekera, and F.P. Zamborini: The synthesis and fabrication of one-dimensional nanoscale heterojunctions. *Small* **3,** 722 (2007).

7. G.C. Liang, J. Xiang, N. Kharche, G. Klimeck, C.M. Lieber, and M. Lundstrom: Performance analysis of a Ge/Si core/shell nanowire field-effect transistor. *Nano Lett.* **7,** 643 (2007).
8. C.Y. Kuan, J.M. Chou, I.C. Leu, and M.H. Hon: Self-organized Zn/ZnO core-shelled hierarchical structures prepared by aqueous chemical growth. *J. Mater. Res.* **23,** 1163 (2008).
9. S.J. An and G.C. Yi: Near ultraviolet light emitting diode composed of n-GaN/ZnO coaxial nanorod heterostructures on a p-GaN layer. *Appl. Phys. Lett.* **91,** 123109 (2007).
10. M. Law, L.E. Greene, A. Radenovic, T. Kuykendall, J. Liphardt, and P.D. Yang: ZnO–Al_2O_3 and ZnO–TiO_2 core-shell nanowire dye-sensitized solar cells. *J. Phys. Chem. B* **110,** 22652 (2006).
11. N. Du, H. Zhang, B.D. Chen, J.B. Wu, and D.R. Yang: Low-temperature chemical solution route for ZnO based sulfide coaxial nanocables: General synthesis and gas sensor application. *Nanotechnology* **18,** 115619 (2007).
12. O. Kazakova, B. Daly, and J.D. Holmes: Tunable magnetic properties of metal/metal oxide nanoscale coaxial cables. *Phys. Rev. B* **74,** 184413 (2006).
13. L. Li, Y.W. Yang, G.H. Li, and L.D. Zhang: Conversion of a Bi nanowire array to an array of Bi–Bi_2O_3 core-shell nanowires and Bi_2O_3 nanotubes. *Small* **2,** 548 (2006).
14. Z.Y. Wang, Q.F. Lu, M.G. Kong, and L.D. Zhang: Manipulation of the morphology of semiconductor-based nanostructures from core-shell nanoparticles to nanocables: The case of CdSe/SiO_2. *Chem. Eur. J.* **13,** 1463 (2007).
15. J.Y. Bae, J.Y. Yoo, and G.C. Yi: Fabrication and photoluminescent characteristics of ZnO/$Mg_{0.2}Zn_{0.8}O$ coaxial nanorod single quantum well structures. *Appl. Phys. Lett.* **89,** 173114 (2006).
16. C.R. Wang, J. Wang, Q. Li, and G.C. Yi: Fabrication and photoluminescent characteristics of ZnO/$Mg_{0.2}Zn_{0.8}O$ coaxial nanorod single-quantum-well structures. *Adv. Funct. Mater.* **15,** 1471 (2005).
17. X.H. Sun, T.K. Sham, R.A. Rosenberg, and G.K. Shenoy: One-dimensional silicon-cadmium selenide heterostructures. *J. Phys. Chem. C* **111,** 8475 (2007).
18. R.Y. Li, X.C. Sun, X.R. Zhou, M. Cai, and X.L. Sun: Aligned heterostructures of single-crystalline tin nanowires encapsulated in amorphous carbon nanotubes. *J. Phys. Chem. C* **111,** 9130 (2007).
19. C.H. Liang, G.W. Meng, L.D. Zhang, N.F. Shen, and X.Y. Zhang: Carbon nanotubes filled partially or completely with nickel. *J. Cryst. Growth* **218,** 136 (2000).
20. B. Deng, A.W. Xu, G.Y. Chen, R.Q. Song, and L.P. Chen: Synthesis of copper-core/carbon-sheath nanocables by a surfactant-assisted hydrothermal reduction/carbonization process. *J. Phys. Chem. B* **110,** 11711 (2006).
21. T. Luo, L.Y. Chen, K.Y. Bao, W.C. Yu, and Y.T. Qian: Solvothermal preparation of amorphous carbon nanotubes and Fe/C coaxial nanocables from sulfur, ferrocene, and benzene. *Carbon* **44,** 2844 (2006).
22. H.S. Qian, S.H. Yu, L.B. Luo, J.Y. Gong, L.F. Fei, and X.M. Liu: Synthesis of uniform Te@carbon-rich composite nanocables with photoluminescence properties and carbonaceous nanofibers by the hydrothermal carbonization of glucose. *Chem. Mater.* **18,** 2102 (2006).
23. L.S. Wang, D.B. Buchholz, Y. Li, J. Li, C.Y. Lee, H.T. Chiu, and R.P.H. Chang: EELS plasmon studies of silver/carbon core/shell nanocables prepared by simple arc discharge. *Appl. Phys. A* **87,** 1 (2007).
24. K.F. Huo, X.M. Zhang, L.S. Hu, X.J. Sun, J.J. Fu, and P.K. Chu: One-step growth and field-emission properties of quasialigned TiO_2 nanowire/carbon nanocone core-shell nanostructure arrays on Ti substrates. *Appl. Phys. Lett.* **93,** 013105 (2008).
25. H.Y. Kim, S.Y. Bae, N.S. Kim, and J. Park: Fabrication of SiC–C coaxial nanocables: Thickness control of C outer layers. *Chem. Commun.* **2634 (2003).**
26. C.Y. Zhi, D.Y. Zhong, and E.G. Wang: GaN-filled carbon nanotubes: Synthesis and photoluminescence. *Chem. Phys. Lett.* **381,** 715 (2003).
27. J.H. Zhan, Y. Bando, J.Q. Hu, Y.B. Li, and D. Golberg: Synthesis and field-emission properties of Ga_2O_3–C nanocables. *Chem. Mater.* **16,** 5158 (2004).
28. L.W. Yin, Y. Bando, Y.C. Zhu, and M.S. Li: Controlled carbon nanotube sheathing on ultrafine InP nanowires. *Appl. Phys. Lett.* **84,** 5314 (2004).
29. S.Y. Bae, H.W. Seo, H.C. Choi, D.S. Han, and J. Park: Single- and double-shelled coaxial nanocables of GaP with silicon oxide and carbon. *J. Phys. Chem. B* **109,** 8496 (2005).
30. X.P. Shen, Z.Y. Jiang, C.L. Gao, Z. Xu, Z.X. Xie, and L.S. Zheng: Controlled carbon nanotube sheathing on ultrafine InP nanowires. *J. Mater. Chem.* **17,** 1326 (2007).
31. E. Sutter, P. Sutter, R. Calarco, T. Stoica, and R. Meijers: Assembly of ordered carbon shells on GaN nanowires. *Appl. Phys. Lett.* **90,** 093118 (2007).
32. M.S. Saha, R.Y. Li, M. Cai, and X.L. Sun: Nanowire-based 3-D hierarchical core/shell heterostructured electrodes for high performance PEM fuel cells. *J. Power Sources* **185,** 1079 (2008).
33. K. Viswanathan and K. Brandt: Crystal-structure and charge carrier concentration of $W_{18}O_{49}$. *J. Solid State Chem.* **36,** 45 (1981).
34. Y.S. Kim, S.C. Ha, K. Kim, H. Yang, S.Y. Choi, Y.T. Kim, J.T. Park, C.H. Lee, J. Choi, J. Paek, and K. Lee: Room-temperature semiconductor gas sensor based on nonstoichiometric tungsten oxide nanorod film. *Appl. Phys. Lett.* **86,** 213105 (2005).
35. J. Polleux, A. Gurlo, N. Barsan, U. Weimar, M. Antonietti, and M. Niederberger: Template-free synthesis and assembly of single-crystalline tungsten oxide nanowires and their gas-sensing properties. *Angew. Chem. Int. Ed.* **45,** 261 (2006).
36. Y.B. Li, Y. Bando, and D. Golberg: Quasi-aligned single-crystalline $W_{18}O_{49}$ nanotubes and nanowires. *Adv. Mater.* **15,** 1294 (2003).
37. S. Jeon and K. Yong: Synthesis and characterization of tungsten oxide nanorods from chemical vapor deposition-grown tungsten film by low-temperature thermal annealing. *J. Mater. Res.* **23,** 1320 (2008).
38. K.Q. Hong, M.H. Xie, R. Hu, and H.S. Wu: Synthesis of tungsten oxide comblike nanostructures. *J. Mater. Res.* **23,** 2657 (2008).
39. J. Polleux, N. Pinna, M. Antonietti, and M. Niederberger: Growth and assembly of crystalline tungsten oxide nanostructures assisted by bioligation. *J. Am. Chem. Soc.* **127,** 15595 (2005).
40. G.Z. Shen, Y. Bando, D. Golberg, and C.W. Zhou: Electron-beam-induced synthesis and characterization of $W_{18}O_{49}$ nanowires. *J. Phys. Chem. C* **112,** 5856 (2008).
41. A. Kawashima, S. Nomura, H. Toyota, T. Takemori, S. Mukasa, and T. Maehara: A supercritical carbon dioxide plasma process for preparing tungsten oxide nanowires. *Nanotechnology* **18,** 495603 (2007).
42. H.H. Hwu and J.G. Chen: Substrate-dependent reaction pathways of ethylene on clean and carbide-modified W(110) and W(111). *J. Phys. Chem. B* **107,** 11467 (2003).
43. G. Gu, B. Zheng, W.Q. Han, S. Roth, and J. Liu: Tungsten oxide nanowires on tungsten substrates. *Nano Lett.* **2,** 849 (2002).
44. A.M. Morales and C.M. Lieber: A laser ablation method for the synthesis of crystalline semiconductor nanowires. *Science* **279,** 208 (1998).
45. S.J. Kwon: Theoretical analysis of non-catalytic growth of nanorods on a substrate. *J. Phys. Chem. B* **110,** 3876 (2006).
46. V.K. Sarin: Morphological changes occurring during reduction of WO_3. *J. Mater. Sci.* **10,** 593 (1975).

47. K.Q. Hong, W.C. Yiu, H.S. Wu, J. Gao, and M.H. Xie: A simple method for growing high quantity tungsten-oxide nanoribbons under moist conditions. *Nanotechnology* **16,** 1608 (2005).
48. Y.Z. Jin, Y.Q. Zhu, R.L.D. Whitby, N. Yao, R.Z. Ma, P.C.P. Watts, H.W. Kroto, and D.R.M. Walton: Simple approaches to quality large-scale tungsten oxide nanoneedles. *J. Phys. Chem. B* **108,** 15572 (2004).
49. J. Pfeifer, E. Badaljan, P. Tekula-Buxbaum, T. Kovacs, O. Geszti, A.L. Toth, and H.J. Lunk: Growth and morphology of $W_{18}O_{49}$ crystals produced by microwave decomposition of ammonium paratungstate. *J. Cryst. Growth* **169,** 727 (1996).
50. A. Rothschild, J. Sloan, and R. Tenne: Growth of WS_2 nanotubes phases. *J. Am. Chem. Soc.* **122,** 5169 (2000).
51. N.A.S.A. Thermo Build: http://cea.grc.nasa.gov.
52. C.H. Ye, X.S. Fang, Y.F. Hao, X.M. Teng, and L.D. Zhang: Zinc oxide nanostructures: Morphology derivation and evolution. *J. Phys. Chem. B* **109,** 19758 (2005).
53. M. Bechelany, A. Brioude, P. Stadelmann, G. Ferro, D. Cornu, and P. Miele: Very long SiC-based coaxial nanocables with tunable chemical composition. *Adv. Funct. Mater.* **17,** 3251 (2007).
54. T.K. Zhao, Y.N. Liu, and J.W. Zhu: Temperature and catalyst effects on the production of amorphous carbon nanotubes by a modified arc discharge. *Carbon* **43,** 2907 (2005).
55. N.Q. Zhao, C.N. He, X.W. Du, C.S. Shi, J.J. Li, and L. Cui: Amorphous carbon nanotubes fabricated by low-temperature chemical vapor deposition. *Carbon* **44,** 1859 (2006).